NIH Public Access
Author Manuscript
J Med Chem. Author manuscript; available in PMC 2014 November 27.

Published in final edited form as:
J Med Chem. 2013 November 27; 56(22): 9242–9250. doi:10.1021/jm401333u.

Discovery of a Potent Inhibitor of Replication Protein A Protein-Protein Interactions Using a Fragment Linking Approach

Andreas O. Frank[1,2,‡,†], **Michael D. Feldkamp**[1,2,‡], **J. Phillip Kennedy**[1,‡], **Alex G. Waterson**[3,4], **Nicholas F. Pelz**[1], **James D. Patrone**[1], **Bhavatarini Vangamudi**[1], **DeMarco V. Camper**[1], **Olivia W. Rossanese**[1], **Walter J. Chazin**[1,2,4], and **Stephen W. Fesik**[1,2,3,4,*]

[1]Department of Biochemistry, Vanderbilt University School of Medicine, Nashville, TN 37232-0146, United States

[2]Center for Structural Biology, Vanderbilt University, Nashville, TN 37232-8725, United States

[3]Department of Pharmacology, Vanderbilt University School of Medicine, Nashville, TN 37232-6600, United States

[4]Department of Chemistry, Vanderbilt University, Nashville, TN 37232-1822, United States

Abstract

Replication protein A (RPA), the major eukaryotic single-stranded DNA (ssDNA) binding protein, is involved in nearly all cellular DNA transactions. The RPA N-terminal domain (RPA70N) is a recruitment site for proteins involved in DNA damage response and repair. Selective inhibition of these protein-protein interactions has the potential to inhibit the DNA damage response and sensitize cancer cells to DNA-damaging agents without affecting other functions of RPA. To discover a potent, selective inhibitor of the RPA70N protein-protein interactions to test this hypothesis, we used NMR spectroscopy to identify fragment hits that bind to two adjacent sites in the basic cleft of RPA70N. High-resolution X-ray crystal structures of RPA70N-ligand complexes revealed how these fragments bind to RPA and guided the design of linked compounds that simultaneously occupy both sites. We have synthesized linked molecules that bind to RPA70N with submicromolar affinity and minimal disruption of RPA's interaction with ssDNA.

INTRODUCTION

RPA is a heterotrimeric single stranded DNA (ssDNA)-binding protein complex composed of 70, 32, and 14 kDa subunits that is essential for eukaryotic DNA replication, damage response, and repair.[1,2] When DNA lesions are encountered at a replication fork, an excess of ssDNA is created that is rapidly coated by RPA.[3] This event initiates signaling to recruit and assemble DNA damage response proteins at DNA damage sites, activate checkpoint pathways, and halt the cell cycle while DNA repair occurs.[4–6] Checkpoint pathways are up-

*Corresponding author: stephen.fesik@vanderbilt.edu, 615-322-6303.
†Current address: Novartis Institutes for BioMedical Research (NIBR), Global Discovery Chemistry, Emeryville, California 94608, United States.
‡These authors contributed equally to this work.

[i]Modeling of a very slightly different alternative position of compound **8** was possible due to the high resolution at which this structure was determined (see Supporting Figure 1).

ASSOCIATED CONTENT

Supporting Information Available: Overlay of the two solutions for the X-ray co-crystal structure of compound **8**. This material is available free of charge via the Internet at http://pubs.acs.org.

PDB ID Codes. The structures of compounds bound to RPA70N E7R have been deposited in the Protein Data Bank under accession codes 4LWC, 4LUV, 4LWI, 4LUZ, and 4LUO.

NIH-PA Author Manuscript
NIH-PA Author Manuscript
NIH-PA Author Manuscript

NIH-PA Author Manuscript

NIH-PA Author Manuscript

NIH-PA Author Manuscript

regulated in multiple cancer types that exhibit higher levels of replicative stress than normal cells.[6–8] In addition, DNA damage response and repair is stimulated in patients by treatment with radiation and/or chemotherapeutic agents, which contributes to resistance to cancer treatment.[9] Correspondingly, there is a growing interest in the inhibition of checkpoint pathways in patients undergoing these treatments.[10–12]

ATR (ATM and Rad3 related) kinase is a major regulator of the DNA damage response. ATR is recruited to sites of DNA damage via the binding of its obligate co-factor ATRIP (ATR Interacting Protein) to the N-terminal domain of the 70 kDa subunit of RPA (RPA70N).[5] Inhibition of the interaction of RPA70N with ATRIP inhibits this recruitment.[10,13] RPA70N utilizes a common basic cleft to bind ATRIP and a number of other partner proteins, including RAD9, MRE11, and p53.[10] Since these interactions are important for mediating the DNA damage response, their inhibition may serve as a potential target for new cancer therapies. However, because RPA also has critical scaffolding functions, traditional knock-down strategies, such as RNAi, are not suitable for validation of this hypothesis. Specific inhibition of RPA70N function with small molecule probes would enable a further understanding and validation of the role of RPA70N-mediated signaling in supporting cancer cell growth and mediating resistance to chemotherapeutics.

High throughput and virtual screening have previously been applied to identify small molecules that bind to RPA and inhibit some of its biochemical activities. However, the molecules discovered thus far exhibit relatively weak binding affinities to RPA70N.[14–18] Traditional high throughput screening has met with relatively limited success for some target classes.[19] In contrast, fragment-based screening[20,21] has shown promise for the generation of small molecule inhibitors of protein-protein interactions.[22–24] Using these methods, our group has previously reported the discovery of compounds that bind to RPA70N with affinities as low as 11 μM and X-ray crystal structures that reveal how they bind to the protein.[25]

Here, we describe the discovery of a new class of potent submicromolar inhibitors of the RPA70N/ATRIP interaction using a fragment screening and linking strategy (SAR by NMR[21]). An NMR-based fragment screen identified low molecular weight compounds that bind to two distinct sites in the basic cleft of RPA70N. High-resolution crystallography revealed the binding modes of the fragments and suggested a strategy for fragment optimization and linking. Medicinal chemistry was employed to improve an initial linked molecule into a compound that binds to RPA70N with submicromolar affinity without interfering with the interaction between RPA70 and ssDNA.

RESULTS

Identification of fragment hits and preliminary SAR

To identify small molecules that bind to RPA70N, we conducted an NMR-based screen of our fragment library (Table 1). The $^{1}H,^{15}N$ HMQC NMR spectrum of RPA70N is well resolved, and the chemical shift assignments are known.[10,26] After exclusion of fragment hits with unfavorable functionality and/or evidence of non-specific binding to the protein, 149 confirmed hits were identified, each of which caused significant chemical shift differences (more than one amide signal line width) at a ligand concentration of 800 μM. The observed hit rate of 1% is slightly lower than prior findings from screening targets involved in protein-protein interactions, but confirms the ligandability of RPA70N.[27,28]

Upon the addition of fragments, NMR chemical shift perturbations were observed for several residues within the basic cleft of RPA70N, including Ser55 (Figure 1A) and Thr60 (Figure 1B), which are located at opposite ends of the cleft. We observed that binding of

NIH-PA Author Manuscript

NIH-PA Author Manuscript

NIH-PA Author Manuscript

some fragments induced independent chemical shift changes for both residues, indicating the likelihood of two different binding sites in the cleft. Indeed, fitting of the chemical shift changes for Ser55 or Thr60 over the course of titrations indicated the binding location(s) of the fragments and provided independent binding affinities for the two distinct sites. Binding constants were obtained for the 81 compounds that demonstrated the largest changes in chemical shift, and fragments were ranked based on their site-specific target affinities and corresponding ligand efficiencies (LEs[29,30]). A summary of the results from this NMR-based fragment screen is given in Table 1. Fragment hits were found to have binding affinities ranging from 490 μM to >2000 μM, with corresponding LEs as high as 0.35. The fragment hits were grouped into chemical series that share a number of structural similarities. Representative examples of the fragment hits are shown in Figure 2. Distinct structural preferences were found for some of the chemical series, an early indication of the presence of SAR that may be exploited for the design of compounds with better binding affinities.

A diverse set of compounds induced chemical shift changes of Ser55 in Site-1. One major cluster of these fragments is a set of carboxylic acid-containing 5/6 fused bicyclic ring systems. One of the most potent examples of this class (although not the most ligand efficient) is the substituted indole **1**. Also in this set is a previously reported chlorobenzthiophene fragment hit.[25] In general, halogen substitutions, particularly chlorine atoms on the heterocyclic core, improve the binding affinity of these molecules. Another notable group of hits that cause chemical shift perturbations of Ser55 is a large set of related fragments that contain a 5-phenylfuran-2-carboxylic acid or related 5-phenylthiophene-2-carboxylic acid motif, as exemplified by **2**. Fragments in this series with the best affinities possess meta-substituted phenyl rings and bind to RPA70N with affinities as low as 710 μM, as determined by NMR-based titrations. General trends in this class of fragment hits include higher binding affinities for furan-containing compounds versus thiophene-based compounds and a requirement for a carboxylic acid for tight binding. While most of the Site-1 fragment hits possess a carboxylic acid, as might be expected for a binding site containing many basic residues, acid isosteres are also represented (e.g. phenyl tetrazole **3**). In general, however, the non-carboxylic acid containing compounds bind with weaker affinity than the acids.

Much less overall diversity was observed among compounds that bind to Site-2. The SAR at this site is dominated by a chemical motif in which a phenyl ring is bound to a five-membered heterocycle with an attached carboxylic acid (Figure 2). Indeed, the fragments with the best affinity and ligand efficiency at Site-2 fit into this chemotype. This motif is exemplified by pyrazole **5**, which binds selectively to Site-2. The phenyl furans, such as **2**, also fit this motif. In general, the binding affinity to Site-2 is improved by meta or para substitutions on the phenyl ring. In particular, methyl and methoxy substitutions are optimal, although halogens are tolerated as well. Selected compounds possess alternate ring systems, such as napthylene and furan rings, in place of the phenyl moiety. Compound **6** represents a rare example of a Site-2 fragment hit that does not have a carboxylic acid. Although some series (for example, the phenyl pyrazoles) bind selectively to one site, many of the hits identified in the screen bind to both sites. In general, these compounds bind to Site-1 more strongly than Site-2 (e.g. fragment **2**).

Using information from our fragment hits as a guide, we engaged in a program of focused purchasing from commercial vendors. Our goal was to explore and expand on the initial SAR, combine features from different fragment hits to produce new chemical series, and to obtain binding affinity improvements. One result of this effort was the creation of a series of recently described RPA70N inhibitors.[25] A second result was the generation of a diphenylpyrazole series (e.g. **4**). Although the design of this series was based on the

NIH-PA Author Manuscript

NIH-PA Author Manuscript

NIH-PA Author Manuscript

pyrazole-containing compounds that bind selectively to Site-2 (e.g. **5**), compound **4** was found to bind more tightly to Site-1, with a K_d of 580 μM. The molecule also induced significant shifts of Thr60, but has a relatively weak K_d for this site (Figure 2).

Determination of binding modes from X-ray structures of RPA70N/ ligand complexes

We have already established that high resolution X-ray crystallographic analysis can be used to determine structures of small molecules with RPA70N, taking advantage of a surface engineered RPA70N E7R mutant.[25,31] In total, co-crystal structures have been obtained for 12 fragment hits. As noted above, many of the fragment hits were determined by NMR to bind to two sites in the basic cleft (Figure 3A), and X-ray crystallography verified this finding.

Fragment hit **2** binds to Site-1 with a K_d of 710 μM and to Site-2 with a K_d of 1400 μM. The crystal structure of the compound in complex with RPA70N revealed binding interactions in both sites (Figure 3B). The halogen-substituted phenyl ring of **2** occupies a relatively small Site-1 pocket, which is defined by residues Ile33, Arg31, Arg43, Ser55, Met57, Leu87, Arg91 and Val93. This pocket is mainly hydrophobic, with positively charged residues situated near its rim. In addition to hydrophobic packing interactions, the 2-furan carboxylic acid forms salt bridges and/or hydrogen bonding interactions with Arg31 and Arg43. Compound **2** also binds to Site-2 and lays flat across a hydrophobic surface of the cleft in a region that is devoid of significant pockets for fragment insertion. In this binding pose, the phenyl ring points toward Site-1, while the 2-furan carboxylic acid forms interactions with the sidechains of Arg41 and Thr60 as well as an extended series of crystallographic water molecules.

Compound **4** was also observed to bind in both sites (Figure 3C). However, the binding pose at Site-2 had less well-defined electron density compared to Site-1, possibly reflecting the weak binding affinity shown for this site in the NMR titrations (>2000 μM). In Site-1, the pyrazole 1-phenyl ring occupies the hydrophobic pocket, while the pyrazole carboxylic acid engages in polar contacts with Arg 31 and Arg 43 in a fashion similar to compound **2**. The 5-phenyl ring of the molecule extends down the basic cleft, above Met 57, pointed directly toward Site-2.

To guide a fragment linking strategy, we also obtained a crystal structure of RPA70N in a ternary complex with compounds **2** and **4** (Figure 3D). As anticipated, compound **4**, which displays better binding affinity to Site-1, occupies this site in a mode similar to its pose when binding alone. Likewise, fragment **2** was found to bind to Site-2 in a manner identical to that described above, except for the position of the chlorine atom. In the ternary structure, a distance of 4.9 Å was observed between the closest heavy atoms in each of the molecules, suggesting that linking the two compounds should be possible.

Construction, optimization and characterization of linked compounds

Examination of the crystal structure of the ternary complex (Figure 3D) revealed that the distance between the 4-position of the phenyl ring of fragment **2** and the 4-position of the 5-pyrazole phenyl ring of compound **4** represents the closest approach of the molecules. Based on this structural information, we designed a short, flexible, two-atom ether-based linker to connect the molecules at these positions (Figure 4). Due to chemical tractability considerations, we chose not to incorporate the chlorine atom of **2** for an initial fragment linking attempt. Compound **7** was synthesized using the methods shown in Scheme 1. The methoxy of the known pyrazole **9** was deprotected using BBr_3 to give phenol **10**. In parallel, the commercially available **11** was brominated using NBS and subsequently used in a simple base-mediated alkylation to afford the ether-linked compound.

NIH-PA Author Manuscript

NIH-PA Author Manuscript

NIH-PA Author Manuscript

The linked compound displays an NMR-derived binding affinity of 26 μM, a dramatic improvement over the individual fragments. This compound was also assessed in an ATRIP-based FPA assay.[32] A comparable binding affinity of 20 μM was calculated[39,40] from IC_{50}s determined from changes in anisotropy as a result of displacement of a labeled peptide probe. While the linked compound produced a >20-fold increase in affinity with respect to the starting fragments, it failed to achieve the potency predicted by the product of the binding affinities of the two fragments[33] (580 μM for **4** × 1870 μM for the des Cl version of **2** = 1.0 μM).

Examination of an X-ray crystal structure of **7** in complex with RPA70N suggested the possible structural reasons for the suboptimal binding affinity (Figure 5A). While the molecule maintained many of the interactions between the individual fragment molecules and the protein, the 5-position phenyl ring of the pyrazole ring was shifted with respect to the binding position of the original fragment (Figure 5C). To improve the binding characteristics of the linked molecule, we used a structure-guided optimization approach to exploit unused space in the basic cleft, particularly in the Site-1 hydrophobic pocket, while maintaining key electrostatic contacts. We also modified the linker, with the intention of adding rigidity, optimizing the linking geometry, and introducing additional interactions in the center of the cleft. These efforts ultimately resulted in lead compound **8** (Figure 4). The synthesis of this elaborated compound hinges upon an amide coupling using amine **16** and acid **19**. Amine **19** was synthesized in two steps beginning with the condensation of hydrazine **13** and dioxobutanoate **14**. This was followed by a Raney nickel mediated reduction of the cyano moiety to give **16** as a methyl ester. The acid coupling partner **19** was formed from the palladium mediated coupling of bromide **17** and furan **18** and then used in an EDC driven amide bond formation reaction. After saponification of **20**, **22** was generated in 20% yield. Alternately, the crude amide was converted to the corresponding thioamide **21** by the action of Lawesson's reagent. Saponification of both esters gave the final compound **8**.

The optimized molecule **8**, which binds to RPA70N with an FPA-derived K_d of 190 nM and has a ligand efficiency of 0.23, features a longer three atom linker and the incorporation of the chlorine atom from the original fragment **2**. Importantly, the two chlorine atoms added to the pyrazole N-phenyl ring recapitulate the optimized Site-1 interactions previously reported for a different series of RPA70N inhibitors[25] (Figure 5B). The X-ray crystal structure of **8** in complex with RPA70N confirms that the chlorine substitutions lead to a more fully occupied Site-1 (Figure 5B and 5D).[i] In addition, the phenyl furan chlorine fills in space above Met57, and the sulfur from the thioamide linker occupies a small lipophilic space under Leu87. The placement of this sulfur atom was critical, as small variations, including amide variants and alternate positioning of the thioamide within the linker led to significant decreases in binding affinity. For example, the corresponding amide **22** displayed a binding affinity of 2.9 μM and a correspondingly reduced LE of 0.18. These three changes result in significant additional hydrophobic contacts within the basic cleft of RPA70N, as well as potentially superior binding geometry, and led to a corresponding improvement in binding affinity and ligand efficiency for compound **8** relative to compound **7**.

The basic cleft of RPA70N is one of four OB-fold domains present in RPA70. The other three bind to ssDNA, with the A and B domains constituting the primary high affinity element of the DNA-binding core.[1] These domains have the potential to influence binding of the compounds to the N-terminal domain through competitive binding or allosteric effects.[14] To address this, we tested the binding of compound **8** to RPA70NAB, a protein construct which contains RPA70N and the adjacent tandem ssDNA-binding domains A and B. Compound **8** binds to RPA70NAB with an FPA-derived K_d of 0.29 μM, similar to its affinity to RPA70N alone, indicating that the presence of additional A and B domains of

NIH-PA Author Manuscript

NIH-PA Author Manuscript

NIH-PA Author Manuscript

RPA have a negligible effect on compound binding to the N-terminal domain and they do not compete significantly with RPA70N for compound **8** (Figure 6).

Our goal is to disrupt the signaling function of RPA70N while leaving the ssDNA-binding functions of RPA intact. To test the functional selectivity of our compounds, we examined the ability of compound **8** to displace a labeled ssDNA probe from the high affinity RPA70 A and B domains. RPA70AB and RPA70NAB, which bind ssDNA with a average K_d of 25 and 10 nM, respectively, were used in an FPA-based competition assay similar to that used above for investigating the displacement of ATRIP from RPA70N (Figure 6). We observed that compound **8** displaced the ssDNA probe only at concentrations 10- to 20-fold higher than that required for the displacement of ATRIP from RPA70N. Indeed, the FPA-derived binding constants from these assays demonstrate that **8** binds more weakly to the ssDNA-binding OB folds of RPA70AB (average K_d = 5.2 μM) or RPA70NAB (average K_d = 2.3 μM) than it does to the RPA70N domain (average K_d = 0.19 μM). Thus, compound **8** exhibits selectivity for binding to the RPA70N domain compared with the ssDNA-binding OB-folds of RPA.

CONCLUSIONS

Protein-protein interactions represent a number of potentially important points of intervention for cancer therapeutics. However, the inhibition of these interactions with small molecules to create drugs or chemical probes remains a difficult endeavor. Based on its involvement in the initiation of critical DNA damage response pathways, RPA is one such target. We have discovered a potent inhibitor of RPA70N-mediated protein-protein interactions using NMR-based fragment screening and a structure-guided linking strategy. The best compound binds to RPA70N with submicromolar affinity and displaces a peptide derived from an endogenous RPA binding partner. In addition, the compound does not substantially perturb the binding of RPA to ssDNA at concentrations needed for inhibition of RPA70N protein-protein interactions. Hence, this series of compounds serves as a lead for generating small molecule probes of selective RPA70N inhibition. The discovery of small molecule probes inhibiting the protein-protein interactions mediated by RPA70N would enable experiments to investigate the role of RPA in cancer biology and may provide a viable foundation for a cancer drug discovery program that targets RPA70N.

EXPERIMENTAL DETAILS

RPA70N Expression and Purification

RPA70N ($RPA_{1–120}$ and the E7R mutant) were produced as described previously with minor modifications.[31,32] Briefly, protein was expressed in BL21-DE3 cells (New England Biolabs) and purified using a Ni Sepharose column (GE Healthcare). Following His tag cleavage and a re-pass over a Ni column to remove the cleaved $(His)_6$ tag, RPA70N was obtained at greater than 95% purity as judged by sodium dodecyl sulfate polyacrylamide gel electrophoresis (SDS–PAGE) analysis. ^{15}N-labeled RPA70N for NMR studies was produced as described, using M9 medium containing 0.5 g of $^{15}NH_4Cl$/L as the sole nitrogen source during growth. RPA70AB and RPA70NAB were produced as described previously.[34]

Fragment Library

Our fragment library consists of a diverse collection of ~15,000 molecules assembled from the commercial collections of a number of vendors and further supplemented with novel compounds synthesized in-house. Compounds were purchased if they passed criteria related to the commonly used “Rule of 3”.[35] Compounds were removed from consideration if they

NIH-PA Author Manuscript

NIH-PA Author Manuscript

NIH-PA Author Manuscript

possessed a molecular weight greater than 250, a cLogP greater than 3.0, more than three hydrogen bond donors or acceptors, and less than four rotatable bonds. Some allowance for exceptions to this rule was made for compounds that represented preferred structures for protein-protein interaction binders.[36] In addition, compounds were required to pass a filter designed to remove fragments containing reactive intermediates and functional groups that were either considered unstable, promiscuous, or poorly soluble.[37] All fragments were prepared as 200 mM d_6-DMSO stock solutions and plated as 12-compound mixtures (20 mM final concentration per molecule) in Matrix 96-well plates.

NMR Spectroscopy

All NMR studies were performed on Bruker Advance III 500 MHz or 600 MHz NMR spectrometers equipped with 5 mm single axis z gradient, inverse cryogenic probes and automatic sample changing systems (Bruker Sample Jet). The fragment library was screened at a temperature of 298 K by recording band-selective, optimized flip angle short transient, $^{1}H,^{15}N$ heteronuclear multiple-quantum coherence (SOFAST-HMQC)[38] and one-dimensional proton-observed spectra. 1D NMR spectra were used to inspect the integrity and behavior of the fragments. Degraded and insoluble compounds, as well as aggregation-mediated binders, were removed from consideration as hits. For all 2D experiments, 1024 data points were recorded in the direct proton, 96 points in the indirect nitrogen dimension and a longitudinal recycle delay of 200 ms was applied. Fully deuterated DMSO was used as a lock signal. The concentration of uniformly ^{15}N-labeled RPA70N was 40 μM, and the fragment concentrations were 800 μM. In total, 14,976 fragments were tested for their binding affinity to RPA70N on the basis of chemical shift perturbations in 2D-HMQC spectra. Mixture hits were subsequently deconvoluted to identify the individual fragments with detectable RPA70N affinity. For titration studies, the protein concentration of 40 μM was kept constant, and the ligand concentration was stepwise increased from 40 μM up to 1200 μM (6-point titrations). ^{1}H and ^{15}N backbone NMR assignments for RPA70N have been reported elsewhere.[10,26] NMR screening and titration data were analyzed with the programs Topspin 2.1 (Bruker AG, Germany) and an in-house software package that applies the expressions of Wang[39,40] for curve fitting.

X-ray Crystallography

Crystals of the E7R mutant of RPA70N were grown as described previously.[31] X-ray diffraction data were collected at sector 21 (Life Sciences Collaborative Access Team, LS-CAT) of the Advanced Photon Source (Argonne, Illinois). All data were processed by HKL-2000.[41] E7R crystallized in space group $P2_12_12_1$ and contained one molecule in the asymmetric unit. Initial phases were obtained by molecular replacement with PHASER[42] using the structure of the free protein (4IPC) as a search model. Iterative cycles of model building and refinement were performed using COOT[43] and PHENIX.[44] The structures of compounds bound to E7R are deposited in the Protein Data Bank under accession codes 4LWC, 4LUV, 4LWI, 4LUZ, and 4LUO. The programs Pymol (Schrödinger, USA) and MOE (Chemical Computing Group Inc., Canada) were used to visualize and analyze the structures.

Organic Synthesis

All NMR spectra for compound characterization were recorded on a Varian Inova 400 (400 MHz NMR spectrometer) located in the small molecule NMR facility at Vanderbilt University. ^{1}H chemical shifts (δ) are reported in ppm values downfield from TMS as the internal standard. Data are reported as follows: chemical shift, multiplicity, coupling constants (Hz), and integration. Apparent splitting patterns are designated as s (singlet), d (doublet), t (triplet), q (quartet), m (multiplet), and br (broad). ^{13}C chemical shifts are reported in δ values in ppm. Low-resolution mass spectra were obtained on an Agilent 1200

NIH-PA Author Manuscript

NIH-PA Author Manuscript

NIH-PA Author Manuscript

LCMS with electrospray ionization. High-resolution mass spectra were recorded on a Waters Qtof API-US plus Acquity system. Analytical thin layer chromatography was performed on 250 mM silica gel 60 F254 plates. Analytical HPLC was performed on an Agilent 1200 analytical LCMS with UV detection at 214 nm and 254 nm along with ELSD detection. Flash column chromatography was performed on silica gel (230–400 mesh, Merck) or using automated silica gel chromatography (Isco, Inc. 100sg Combiflash).

5-(4-Hydroxyphenyl)-1-(*m*-tolyl)-1*H*-pyrazole-3-carboxylic acid (10)

To a flask containing pyrazole **9** (1.0 g, 2.97 mmol, 1 equivalent) under an argon atmosphere was added anhydrous DCM (50 mL) and the mixture was cooled to 0°C. To this was added BBr_3 (14.9 mL, 1.0M in DCM, 5 equivalent.) and the reaction was stirred for 2 hours. Once determined complete by LCMS, the reaction was quenched with 100 mL of H_2O, concentrated, and washed 2× with 200 mL Et_2O to give 0.54 g (62%) of **10**, >98% pure by LC analysis at 214 nm. ^{1}H-NMR (400 MHz, d_6-DMSO): δ 7.28 (m, 3H), 7.06 (d, *J* = 8.0 Hz, 2H), 7.01 (d, *J* = 8.0 Hz, 1H), 6.92 (s, 1H), 6.72 (d, *J* = 8.0 Hz, 2H), 2.32 (s, 3H); ^{13}C NMR (100 MHz, d_6-DMSO): δ 163.5, 158.2, 144.8, 144.5, 139.8, 139.2, 130.3, 129.4, 129.2, 126.3, 123.0, 120.1, 115.8, 109.1, 21.2; HRMS [M + H^+] calcd for $C_{17}H_{15}N_2O_3$ 295.1083; found: 295.1082.

5-(4-(Bromomethyl)phenyl)furan-2-carboxylic acid (12)

To a flask containing furan **11** (1.0 g, 4.9 mmol, 1 equivalent) was added CCl_4 (100 mL), AIBN (80 mg, 4.9 mmol, 0.1 equivalent), NBS (0.92 g, 5.4 mmol, 1.1 equivalent.) and the reaction mixture was heated to reflux for 48h. Once reaction determined to be complete by LCMS, reaction was concentrated to half volume and solid product was collected by filtration to afford 1.2 g (87%) of **12**, >98% pure by LC analysis at 214 nm. ^{1}H-NMR (400 MHz, d_6-DMSO): δ 7.81 (d, *J* = 8.0 Hz, 2H), 7.56 (d, *J* = 8.0 Hz, 2H), 7.33 (d, *J* = 4.0 Hz, 1H), 7.18 (d, *J* = 4.0 Hz, 1H), 4.76 (s, 2H). ^{13}C NMR (100 MHz, d_6-DMSO): δ 178.7, 143.2, 138.9, 130.5, 129.2, 125.0, 120.3, 108.7, 34.4. MS (ESI) *m/z* = 280.1 [M + H^+].

5-(4-((4-(5-Carboxyfuran-2-yl)benzyl)oxy)phenyl)-1-(*m*-tolyl)-1*H*-pyrazole-3-carboxylic acid (7)

To a flask containing pyrazole **10** (100 mg, 0.34 mmol, 1 equivalent.) was added DMF (2 mL), and K_2CO_3 (93 mg, 0.6 8mmol, 2 equivalent). To this was added furan **12** (105 mg, 0.34 mmol, 1 equivalent) and the reaction was allowed to stir overnight. Once determined complete by LCMS, the reaction was quenched with 50 mL of 1N HCl and extracted 3× with 50 mL of DCM. The organic layer was dried with $MgSO_4$, filtered, concentrated and purified via HPLC to give 42 mg (25%) of **7**, >98% pure by LC analysis at 214 nm. ^{1}H-NMR (400 MHz, d_6-DMSO): δ 9.78 (br s, 1H), 7.85 (d, *J* = 8.0 Hz, 2H), 7.58 (d, *J* = 8.0 Hz, 2H), 7.33 (d, *J* = 2.0 Hz, 1H), 7.26 (m, 3H), 7.16 (d, *J* = 2.0 Hz, 1H), 7.05 (m, 4H), 6.72 (d, *J* = 8.0 Hz, 2H), 5.40 (s, 2H), 2.31 (s, 3H); ^{13}C NMR (100 MHz, d_6-DMSO): d 161.9, 159.6, 158.3, 156.3, 145.1, 144.6, 143.2, 139.7, 139.3, 137.2, 130.4, 129.4, 129.3, 129.2, 126.4, 124.9, 123.1, 120.3, 119.9, 115.8, 109.2, 108.6, 65.8, 49.0, 21.1; HRMS [M + H^+] calcd for $C_{29}H_{23}N_2O_6$ 495.1556; found: 495.1562.

Ethyl 5-(4-cyanophenyl)-1-(3,4-dichlorophenyl)-1*H*-pyrazole-3-carboxylate (15)

To a microwave vial containing ketone **14** (1.0 g, 0.0041 mol, 1 equivalent) and hydrazine **13** (0.96 g, 0.0045 mol, 1.1 equivalent) was added ethanol (10 mL), and the reaction was heated to 120°C for 30 min. The reaction mixture was concentrated and then purified by flash chromatography to give 1.2 g (76%) of **15**, >98% pure by LC analysis at 214 nm. ^{1}H-NMR (400 MHz, d_6-DMSO): δ 7.89 (d, *J* = 8.4 Hz, 2H), 7.79 (d, *J* = 2.4 Hz, 1H), 7.72 (d, *J* = 8.8 Hz, 1H), 7.52 (d, *J* = 8.4 Hz, 2H), 7.30 (m, 2H), 4.35 (q, *J* = 7.2, 16.0 Hz, 2H), 1.32 (t,

NIH-PA Author Manuscript

NIH-PA Author Manuscript

NIH-PA Author Manuscript

J = 7.2 Hz, 3H); ^{13}C NMR (100 MHz, d_6-DMSO): δ 161.6, 151.2, 144.6, 143.4, 138.8, 133.3, 133.0, 132.2, 131.6, 130.0, 128.1, 126.3, 113.3, 112.9, 111.4, 61.2, 14.6; MS (ESI) *m/z* = 386.0 [M + H$^+$].

Methyl 5-(4-(aminomethyl)phenyl)-1-(3,4-dichlorophenyl)-1*H*-pyrazole-3-carboxylate (16)

To a flask containing nitrile **15** (1.6 g, 0.0041 mol, 1 equivalent), purged 3 times with argon, was added 50 mL of 2M NH_3 in MeOH. To this was added a catalytic amount of Raney Nickel and then the reaction was put under an atmosphere of hydrogen and stirred for 2 hours. Once determined complete by LCMS the reaction was filtered through a pad of celite, washed 3 times with 100 mL MeOH and concentrated to give 1.1 g (71%) of **16**, >98% pure by LC analysis at 214 nm. ^{1}H-NMR (400 MHz, d_6-DMSO): δ 7.75 (d, *J* = 4.0 Hz, 1H), 7.72 (d, *J* = 8.8 Hz, 1H), 7.36 (d *J* = 8.0 Hz, 2H), 7.26 (m, 3H), 7.13 (s, 1H), 3.87 (s, 3H), 3.74 (s, 2H), 3.05 (br s, 2H); ^{13}C NMR (100 MHz, d_6-DMSO): δ 162.2, 145.5, 145.2, 144.1, 139.2, 132.0, 131.7, 131.4, 128.9, 127.9, 127.8, 126.7, 126.1, 110.2, 52.3, 45.4; MS (ESI) *m/z* = 390.1 [M + H$^+$].

2-Chloro-4-(5-(methoxycarbonyl)furan-2-yl)benzoic acid (19)

According to the method of Fu and Doucet,[45] to a microwave vial containing bromide **17** (0.5 g, 0.0021 mol, 1 equivalent), furan **18** (1.07 g, 0.0085 mol, 4 equivalent), potassium acetate (0.834 g, 0.0085 mol, 4 equivalent), and palladium acetate (50 mg, cat.) was added DMA (5 mL), and the reaction flask was heated to 100°C for 30 min in a microwave reactor. Once determined complete by LCMS the reaction mixture was quenched with 100 mL of 1M aqueous HCl, diluted with 200 mL DCM and extracted 2× with 200 mL DCM, dried with $MgSO_4$, filtered and concentrated. The crude reaction mixture was purified by flash chromatography to give 0.24 g (41%) of **19**, >98% pure by LC analysis at 214 nm. ^{1}H-NMR (400 MHz, d_6-DMSO): δ 7.97 (d, *J* = 1.6 Hz, 1H), 7.92 (d, *J* = 8.4 Hz, 1H), 7.84 (dd, *J* = 1.6, 8.4 Hz, 1H), 7.46 (d, *J* = 3.6 Hz, 1H), 7.43 (d, *J* = 3.6 Hz, 1H) 3.86 (s, 3H); ^{13}C NMR (100 MHz, d_6-DMSO): δ 166.5, 158.5, 154.4, 144.4, 133.2, 133.0, 132.4, 131.2, 126.5, 123.2, 120.8, 111.2, 52.4; MS (ESI) *m/z* = 281.0 [M + H$^+$].

5-(4-((4-(5-Carboxyfuran-2-yl)-2-chlorophenylthioamido)methyl)phenyl)-1-(3,4-dichlorophenyl)-1*H*-pyrazole-3-carboxylic acid (8)

To a flask containing amine **16** (47 mg, 0.125 mmol, 1 equivalent.), acid **19** (35 mg, 0.125 mmol, 1 equivalent), HOBt (17 mg, 0.125 mmol, 1 equivalent) and EDC (36 mg, 0.186 mmol, 1.5 equivalent.) was added DMF (1.8 mL) and DIEA (0.2 mL) and the mixture was allowed to stir overnight. Once determined complete by LCMS, the reaction was quenched with 20 mL H_2O, extracted with 20 mL DCM, washed 2× with 20 mL DCM, dried with $MgSO_4$, filtered and concentrated. The crude reaction mixture containing amide 20 was used without further purification.

To a microwave vial containing crude amide **20** (40 mg, 0.0625 mmol, 1 equivalent) was added Lawesson's Reagent (51 mg, 0.125 mmol, 2 equivalent.) and anhydrous THF (1.0 mL). The reaction was heated in a microwave reactor at 140 °C for 30 min. until the reaction was determined complete by LCMS. The reaction was quenched with 20 mL H_2O, extracted with 20 mL DCM, washed 2× with 20 mL DCM, dried with $MgSO_4$, filtered, and concentrated. The crude reaction mixture containing thioamide **21** was used without further purification.

To a microwave vial containing crude thioamide **21** (45 mg, 0.069 mmol, 1 equivalent) was added 2M LiOH (0.2 mL) and THF (0.8 mL) and the reaction was heated at 120 °C for 10 min. Once determined complete by LCMS, the reaction was quenched with 20 mL H_2O, extracted with 20 mL DCM, washed 2× with 20 mL DCM, dried with $MgSO_4$, filtered, and

NIH-PA Author Manuscript

NIH-PA Author Manuscript

NIH-PA Author Manuscript

concentrated. The crude reaction mixture was purified via HPLC to give 12 mg (28%) of **8,** >98% pure by LC analysis at 214 nm. ^{1}H-NMR (400 MHz, d_6-DMSO): δ 11.08 (br s, 1H), 7.90 (d, *J* = 1.6 Hz, 1H), 7.87 (d, *J* = 6.8 Hz, 1H), 7.78 (d, *J* = 6.8 Hz, 1H), 7.78 (d, *J* = 2.4 Hz, 1H), 7.70 (d, *J* = 8.8 Hz, 2H), 7.50 (d, *J* = 8.8 Hz, 2H), 7.32 (m, 3H), 7.26 (dd, *J* = 8.4, 2.2 Hz, 2H), 4.97 (d, *J* = 5.6 Hz, 2H); ^{13}C NMR (100 MHz, d_6-DMSO): δ 195.9, 163.2, 159.5, 154.4, 145.4, 145.2, 144.7, 142.4, 139.3, 138.1, 133.4, 132.7, 132.5, 132.0, 131.6, 131.4, 130.9, 130.0, 129.2, 128.5, 128.0, 127.9, 125.2, 123.1, 115.6, 114.6, 110.1, 55.9; MS (ESI) *m/z* = 626.0 [M + H^+]. HRMS [M + Na^+] calcd for $C_{29}H_{18}N_3O_5SNa$ 647.9930; found: 647.9933.

5-(4-((4-(5-Carboxyfuran-2-yl)-2-chlorobenzamido)methyl)phenyl)-1-(3,4-dichlorophenyl)-1*H*-pyrazole-3-carboxylic acid (22)

Crude **20** (100 mg, 0.160 mmol, 1 equivalent), prepared in the same manner as above, was dissolved in 3 mL of THF and 2M LiOH (1 mL) and stirred 2 hours at rt. Once complete, the reaction was partitioned between 10 mL of H_2O and 10 mL of DCM. The mixture was acidified with 1M HCl until pH = 3, the layers were separated, and the water layer was washed 2× with 10 mL of DCM. The organic layer was dried with $MgSO_4$, filtered, and concentrated. The crude material was purified on reverse phase HPLC to give 20 mg (20%) of **22**, >98% pure by LC analysis at 214nm. ^{1}H-NMR (400 MHz, d_6-DMSO): δ 9.09 (t, *J* = 6.0 Hz, 1H), 7.94 (d, *J* = 1.4 Hz, 1H), 7.81 (dd, *J* = 1.4 Hz, 8.0 hz, 1H), 7.75 (d, *J* = 2.4 Hz, 1H), 7.71 (d, *J* = 8.6 Hz, 1H), 7.59 (d, *J* = 8.6 Hz, 1H), 7.32 (m, 7H), 7.08 (s, 1H), 4.48 (d, *J* = 5.8 Hz, 2H), 3.75 (br s, 2H); ^{13}C NMR (100 MHz, d_6-DMSO): δ 166.0, 162.8, 159.1, 153.9, 145.0, 144.9, 144.4, 140.1, 138.9, 136.4, 131.6, 131.3, 131.2, 131.0, 130.9, 128.8, 127.5, 127.4, 127.1, 125.7, 125.0, 122.7, 119.8, 110.0, 42.1; MS (ESI) *m/z* = 610.0 [M + H^+].

Fluorescence Polarization Anisotropy (FPA) Assays

FPA competition assays were conducted as previously described with minor modifications.[25,32] Briefly, the K_d of the labeled probe for each protein construct was determined; all assays were conducted using a protein concentration equal to this measured K_d. Therefore, competition for binding to RPA70N was measured using either the FITC-ATRIP peptide (50 nM FITC-Ahx-DFTADDLEELDTLAS-NH_2 with 6 μM RPA70N) or the FITC-ATRIP2 peptide (25 nM FITC-Ahx-DFTADDLEEWFAL-NH_2 with 350 nM RPA70N). Binding to RPA70NAB was measured using 200 nM RPA70NAB and 25 nM FITC-ATRIP2. Competition experiments using ssDNA were conducted as previously described[46] using 10 nM FITC-ssDNA with either 25 nM RPA70AB or 10 nM RPA70NAB. Compounds were diluted in a 10-point, 3-fold serial dilution scheme in DMSO for a final concentration range of 500 – 0.025 μM. Compounds were added to assay buffer (50 mM HEPES, 75 mM NaCl, 5 mM DTT, pH 7.5) containing FITC-labeled probe and appropriate RPA70 protein in a final reaction volume of 50 μL containing 5% DMSO. Anisotropy was measured and plotted against compound concentration using a 4-parameter logistic fit to generate an IC_{50}; this value was converted to K_d, as described.[32, 39,40]

Supplementary Material

Refer to Web version on PubMed Central for supplementary material.

Acknowledgments

We would like to thank Dr. David Cortez for his intellectual contributions in the conception of this project and Dr. Ed Olejniczak for his helpful suggestions and critical review of this manuscript.

Funding Sources

NIH-PA Author Manuscript

NIH-PA Author Manuscript

NIH-PA Author Manuscript

Funding of this research was provided in part by NIH grants 5DP1OD006933/8DP1CA174419 (NIH Director' s Pioneer Award) to S.W.F., R01GM065484 to W.J.C., and ARRA stimulus grant (5RC2CA148375) to Lawrence J. Marnett. A.O.F. was supported by a Deutscher Akademischer Austausch Dienst (DAAD) postdoctoral fellowship, M.D.F. by the NIH NRSA postdoctoral fellowship (F32 ES021690-01), and J.P.K. by 5T21CA9582-24 to Scott Hiebert.

ABBREVIATIONS

RPA	Replication Protein A
FPA	Fluorescence Polarization Anisotropy assay
LE	ligand efficiency

REFERENCES

1. Wold MS. Replication protein A: a heterotrimeric, single-stranded DNA-binding protein required for eukaryotic DNA metabolism. Annu. Rev. Biochem. 1997; 66:61–92. [PubMed: 9242902]
2. Wold MS, Kelly T. Purification and characterization of replication protein A, a cellular protein required for in vitro replication of simian virus 40 DNA. Proc. Natl. Acad. Sci. 1988; 85:2523–2527. [PubMed: 2833742]
3. Fanning E, Klimovich V, Nager AR. A dynamic model for replication protein A (RPA) function in DNA processing pathways. Nucleic Acids Res. 2006; 34:4126–4137. [PubMed: 16935876]
4. Cortez D, Guntuku S, Qin J, Elledge SJ. ATR and ATRIP: Partners in checkpoint signaling. Science. 2001; 294:1713–1716. [PubMed: 11721054]
5. Cimprich KA, Cortez D. ATR: an essential regulator of genome integrity. Nat. Rev. Mol. Cell Biol. 2008; 9:616–627. [PubMed: 18594563]
6. Gorgoulis VG, Pratsinis H, Zacharatos P, Demoliou C, Sigala F, Asimacopoulos PJ, Papavassiliou AG, Kletsas D. p53-dependent ICAM-1 overexpression in senescent human cells identified in atherosclerotic lesions. Lab. Invest. 2005; 85:502–511. [PubMed: 15711569]
7. Bartkova J, Rezaei N, Liontos M, Karakaidos P, Kletsas D, Issaeva N, Vassiliou LV, Kolettas E, Niforou K, Zoumpourlis VC, Takaoka M, Nakagawa H, Tort F, Fugger K, Johansson F, Sehested M, Andersen CL, Dyrskjot L, Orntoft T, Lukas J, Kittas C, Helleday T, Halazonetis TD, Bartek J, Gorgoulis VG. Oncogene-induced senescence is part of the tumorigenesis barrier imposed by DNA damage checkpoints. Nature. 2006; 444:633–637. [PubMed: 17136093]
8. Ciccia A, Bredemeyer AL, Sowa ME, Terret ME, Jallepalli PV, Harper JW, Elledge SJ. The SIOD disorder protein SMARCAL1 is an RPA-interacting protein involved in replication fork restart. Gene Dev. 2009; 23:2415–2425. [PubMed: 19793862]
9. Bartkova J, Horejsi Z, Koed K, Kramer A, Tort F, Zieger K, Guldberg P, Sehested M, Nesland JM, Lukas C, Orntoft T, Lukas J, Bartek J. DNA damage response as a candidate anti-cancer barrier in early human tumorigenesis. Nature. 2005; 434:864–870. [PubMed: 15829956]
10. Xu X, Vaithiyalingam S, Glick GG, Mordes DA, Chazin WJ, Cortez D. The Basic Cleft of RPA70N Binds Multiple Checkpoint Proteins, Including RAD9, To Regulate ATR Signaling. Mol. Cell Biol. 2008; 28:7345–7353. [PubMed: 18936170]
11. Shaheen FS, Znojek P, Fisher A, Webster M, Plummer R, Gaughan L, Smith GCM, Leung HY, Curtin NJ, Robson CN. Targeting the DNA Double Strand Break Repair Machinery in Prostate Cancer. Plos One. 2011; 6:e20311. [PubMed: 21629734]
12. Rakha EA, Chan S. Metastatic Triple-negative Breast Cancer. Clin. Oncol. 2011; 23:587–600.
13. Zou L, Elledge SJ. Sensing DNA damage through ATRIP recognition of RPA-ssDNA complexes. Science. 2003; 300:1542–1548. [PubMed: 12791985]
14. Glanzer JG, Carnes KA, Soto P, Liu S, Parkhurst LJ, Oakley GG. A small molecule directly inhibits the p53 transactivation domain from binding to replication protein A. Nucleic Acids Res. 2013; 41:2047–2059. [PubMed: 23267009]
15. Glanzer JG, Liu S, Oakley GG. Small molecule inhibitor of the RPA70 N-terminal protein interaction domain discovered using in silico and in vitro methods. Bioorg. Med. Chem. 2011; 19:2589–2595. [PubMed: 21459001]

NIH-PA Author Manuscript

NIH-PA Author Manuscript

NIH-PA Author Manuscript

16. Andrews BJ, Turchi JJ. Development of a high-throughput screen for inhibitors of replication protein A and its role in nucleotide excision repair. Mol. Cancer Ther. 2004; 3:385–391. [PubMed: 15078981]

17. Shuck SC, Turchi JJ. Targeted inhibition of Replication Protein A reveals cytotoxic activity, synergy with chemotherapeutic DNA-damaging agents, and insight into cellular function. Cancer Res. 2010; 70:3189–3198. [PubMed: 20395205]

18. Anciano Granadillo VJ, Earley JN, Shuck SC, Georgiadis MM, Fitch RW, Turchi JJ. Targeting the OB-Folds of Replication Protein A with Small Molecules. J. Nucleic Acids. 2010; 2010:304035. [PubMed: 21188165]

19. Macarron R. Critical review of the role of HTS in drug discovery. Drug Discov. Today. 2006; 11:277–279. [PubMed: 16580969]

20. Hajduk PJ, Greer J. A decade of fragment-based drug design: strategic advances and lessons learned. Nature Rev. Drug Disc. 2007; 6:211–219.

21. Shuker SB, Hajduk PJ, Meadows RP, Fesik SW. Discovering high-affinity ligands for proteins: SAR by NMR. Science. 1996; 274:1531–1534. [PubMed: 8929414]

22. Petros AM, Huth JR, Oost T, Park CM, Ding H, Wang XL, Zhang HC, Nimmer P, Mendoza R, Sun CH, Mack J, Walter K, Dorwin S, Gramling E, Ladror U, Rosenberg SH, Elmore SW, Fesik SW, Hajduk PJ. Discovery of a potent and selective Bcl-2 inhibitor using SAR by NMR. Bioorg. Med. Chem. Lett. 2010; 20:6587–6591. [PubMed: 20870405]

23. Sun Q, Burke JP, Phan J, Burns MC, Olejniczak ET, Waterson AG, Lee T, Rossanese OW, Fesik SW. Discovery of Small Molecules that Bind to K-Ras and Inhibit Sos-Mediated Activation. Angew. Chem. Int. Ed. Engl. 2012; 51:6140–6143. [PubMed: 22566140]

24. Friberg A, Vigil D, Zhao B, Daniels RN, Burke JP, Garcia-Barrantes PM, Camper D, Chauder BA, Lee T, Olejniczak ET, Fesik SW. Discovery of potent myeloid cell leukemia 1 (Mcl-1) inhibitors using fragment-based methods and structure-based design. J. Med. Chem. 2013; 56:15–30. [PubMed: 23244564]

25. Patrone JDKJP, Frank AO, Feldkamp MD, Vangamudi B, Pelz NF, Rossanese OW, Waterson AG, Chazin WJ, Fesik SW. Discovery of Protein-Protein Interaction Inhibitors of Replication Protein A. ACS Med. Chem. Lett. 2013; 4:601–605. [PubMed: 23914285]

26. Bochkareva E, Kaustov L, Ayed A, Yi GS, Lu Y, Pineda-Lucena A, Liao JCC, Okorokov AL, Milner J, Arrowsmith CH, Bochkarev A. Single-stranded DNA mimicry in the p53 transactivation domain interaction with replication protein A. Proc. Natl. Acad. Sci. 2005; 102:15412–15417. [PubMed: 16234232]

27. Hajduk PJ, Huth JR, Fesik SW. Druggability indices for protein targets derived from NMR-based screening data. J. Med. Chem. 2005; 48:2518–2525. [PubMed: 15801841]

28. Schuffenhauer A, Ruedisser S, Marzinzik AL, Jahnke W, Blommers M, Selzer P, Jacoby E. Library design for fragment based screening. Curr. Top. Med. Chem. 2005; 5:751–762. [PubMed: 16101415]

29. Hopkins AL, Groom CR, Alex A. Ligand efficiency: a useful metric for lead selection. Drug Discov. Today. 2004; 9:430–431. [PubMed: 15109945]

30. Kuntz ID, Chen K, Sharp KA, Kollman PA. The maximal affinity of ligands. Proc. Natl. Acad. Sci. 1999; 96:9997–10002. [PubMed: 10468550]

31. Feldkamp MDFAO, Kennedy JP, Patrone JD, Vangamudi B, Waterson AG, Fesik SW, Chazin WJ. Surface reengineering enables co-crystallization with an inhibitor of the RPA interaction motif of ATRIP. Biochemistry. 2013; 52:6515–6524. [PubMed: 23962067]

32. Souza-Fagundes EM, Frank AO, Feldkamp MD, Dorset DC, Chazin WJ, Rossanese OW, Olejniczak ET, Fesik SW. A high-throughput fluorescence polarization anisotropy assay for the 70N domain of replication protein A. Anal. Biochem. 2012; 421:742–749. [PubMed: 22197419]

33. Ichihara O, Barker J, Law RJ, Whittaker M. Compound Design by Fragment-Linking. Mol. Inform. 2011; 30:298–306.

34. Brosey CA, Chagot ME, Ehrhardt M, Pretto DI, Weiner BE, Chazin WJ. NMR analysis of the architecture and functional remodeling of a modular multidomain protein, RPA. J. Am. Chem. Soc. 2009; 131:6346–6347. [PubMed: 19378948]

NIH-PA Author Manuscript

NIH-PA Author Manuscript

NIH-PA Author Manuscript

35. Congreve M, Carr R, Murray C, Jhoti H. A 'rule of three' for fragment-based lead discovery? Drug Discov. Today. 2003; 8:876–877. [PubMed: 14554012]
36. Hajduk PJ, Bures M, Praestgaard J, Fesik SW. Privileged molecules for protein binding identified from NMR-based screening. J. Med. Chem. 2000; 43:3443–3447. [PubMed: 10978192]
37. Baell JB, Holloway GA. New substructure filters for removal of pan assay interference compounds (PAINS) from screening libraries and for their exclusion in bioassays. J. Med. Chem. 2010; 53:2719–2740. [PubMed: 20131845]
38. Schanda P, Brutscher B. Hadamard frequency-encoded SOFAST-HMQC for ultrafast two-dimensional protein NMR. J. Magn. Reson. 2006; 178:334–339. [PubMed: 16269260]
39. Wang ZX. An exact mathematical expression for describing competitive binding of two different ligands to a protein molecule. FEBS Lett. 1995; 360:111–114. [PubMed: 7875313]
40. Wang ZX, Jiang RF. A novel two-site binding equation presented in terms of the total ligand concentration. FEBS Lett. 1996; 392:245–249. [PubMed: 8774854]
41. Otwinowski ZMW. Processing of X-Ray Diffraction Data Collected in Oscillation Mode. Methods Enzymol. 1997; 276:307–326.
42. Winn MD, Ballard CC, Cowtan KD, Dodson EJ, Emsley P, Evans PR, Keegan RM, Krissinel EB, Leslie AG, McCoy A, McNicholas SJ, Murshudov GN, Pannu NS, Potterton EA, Powell HR, Read RJ, Vagin A, Wilson KS. Overview of the CCP4 suite and current developments. Acta Cryst. 2011; D67:235–242.
43. Emsley P, Cowtan K. Coot: model-building tools for molecular graphics. Acta Cryst. 2004; D60:2126–2132.
44. Adams PD, Afonine PV, Bunkoczi G, Chen VB, Davis IW, Echols N, Headd JJ, Hung LW, Kapral GJ, Grosse-Kunstleve RW, McCoy AJ, Moriarty NW, Oeffner R, Read RJ, Richardson DC, Richardson JS, Terwilliger TC, Zwart PH. PHENIX: a comprehensive Python-based system for macromolecular structure solution. Acta Cryst. 2010; D66(Pt 2):213–221.
45. Fu HY, Doucet H. Methyl 2-Furoate: An Alternative Reagent to Furan for Palladium-Catalysed Direct Arylation. Eur. J. Org. Chem. 2011; 35:7163–7173.
46. Brosey CA, Yan C, Tsutakawa SE, Heller WT, Rambo RP, Tainer JA, Ivanov I, Chazin WJ. A new structural framework for integrating replication protein A into DNA processing machinery. Nucleic Acids Res. 2013; 41:2313–2327. [PubMed: 23303776]

NIH-PA Author Manuscript
NIH-PA Author Manuscript
NIH-PA Author Manuscript

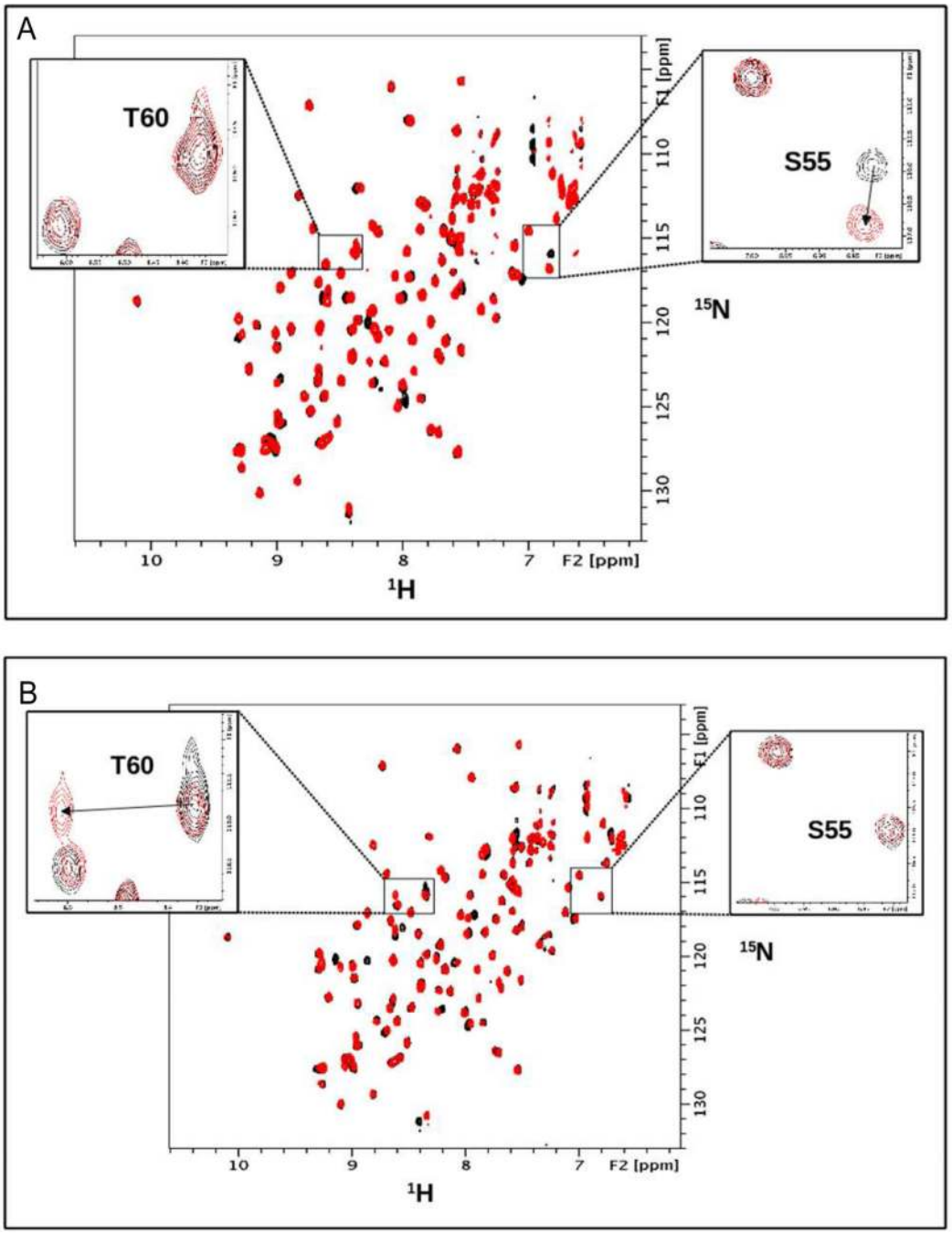

Figure 1.

Overlay of RPA70N $^{1}H,^{15}N$ correlation spectra in the absence (black) and presence (red) of fragment hits. A. Perturbation of Ser55 (S55) reflects binding of a ligand to Site-1 of RPA70N. B. Perturbation of Thr60 (T60) is observed when a fragment binds to Site-2.

NIH-PA Author Manuscript

NIH-PA Author Manuscript

NIH-PA Author Manuscript

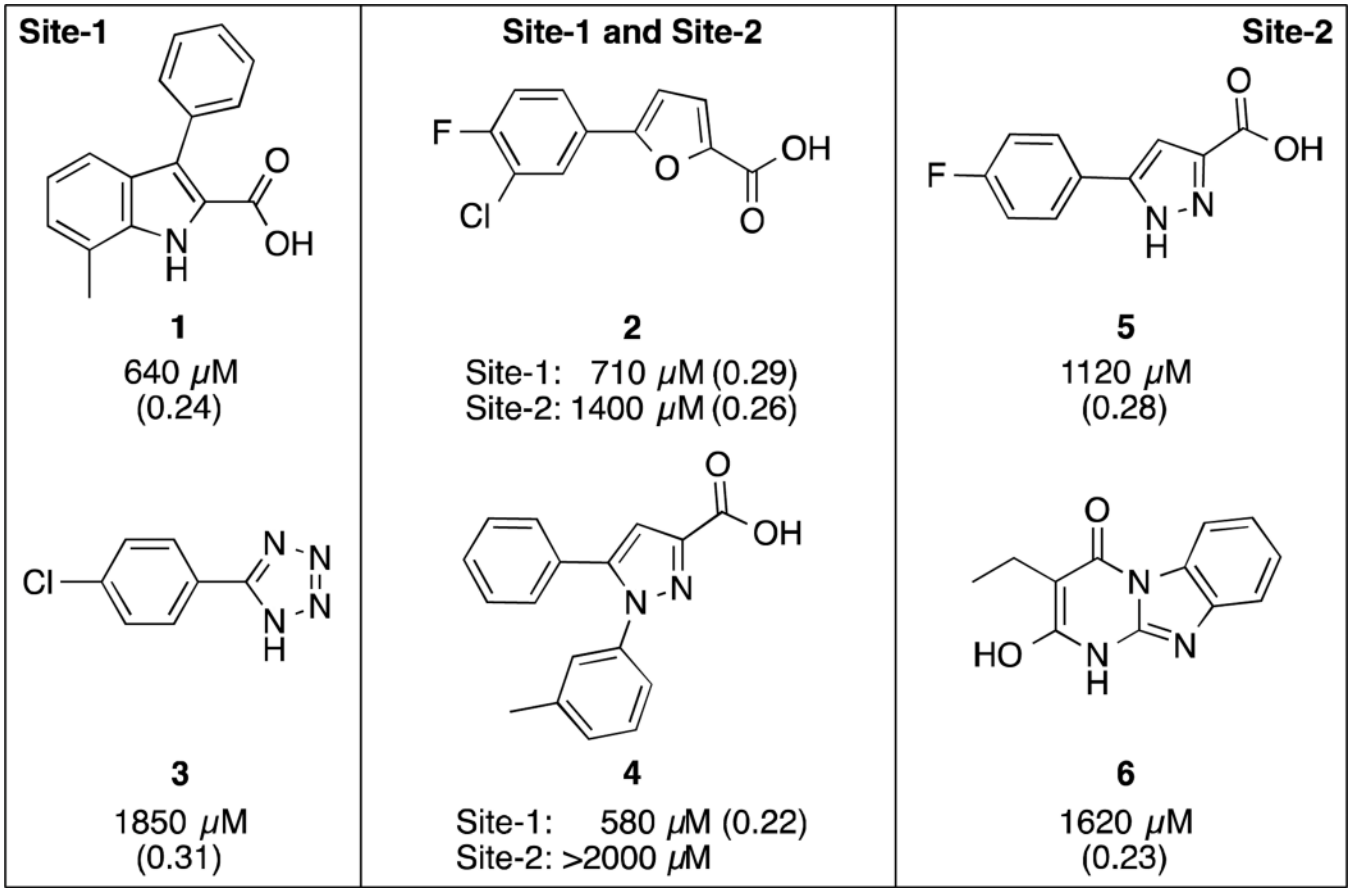

Figure 2.

Selected hits and analogs identified by NMR-based screening. K_ds are listed and ligand efficiencies are in parentheses. Compounds that bind selectively to Site-1 or Site-2 are shown as well as compounds that bind to both sites.

NIH-PA Author Manuscript
NIH-PA Author Manuscript
NIH-PA Author Manuscript

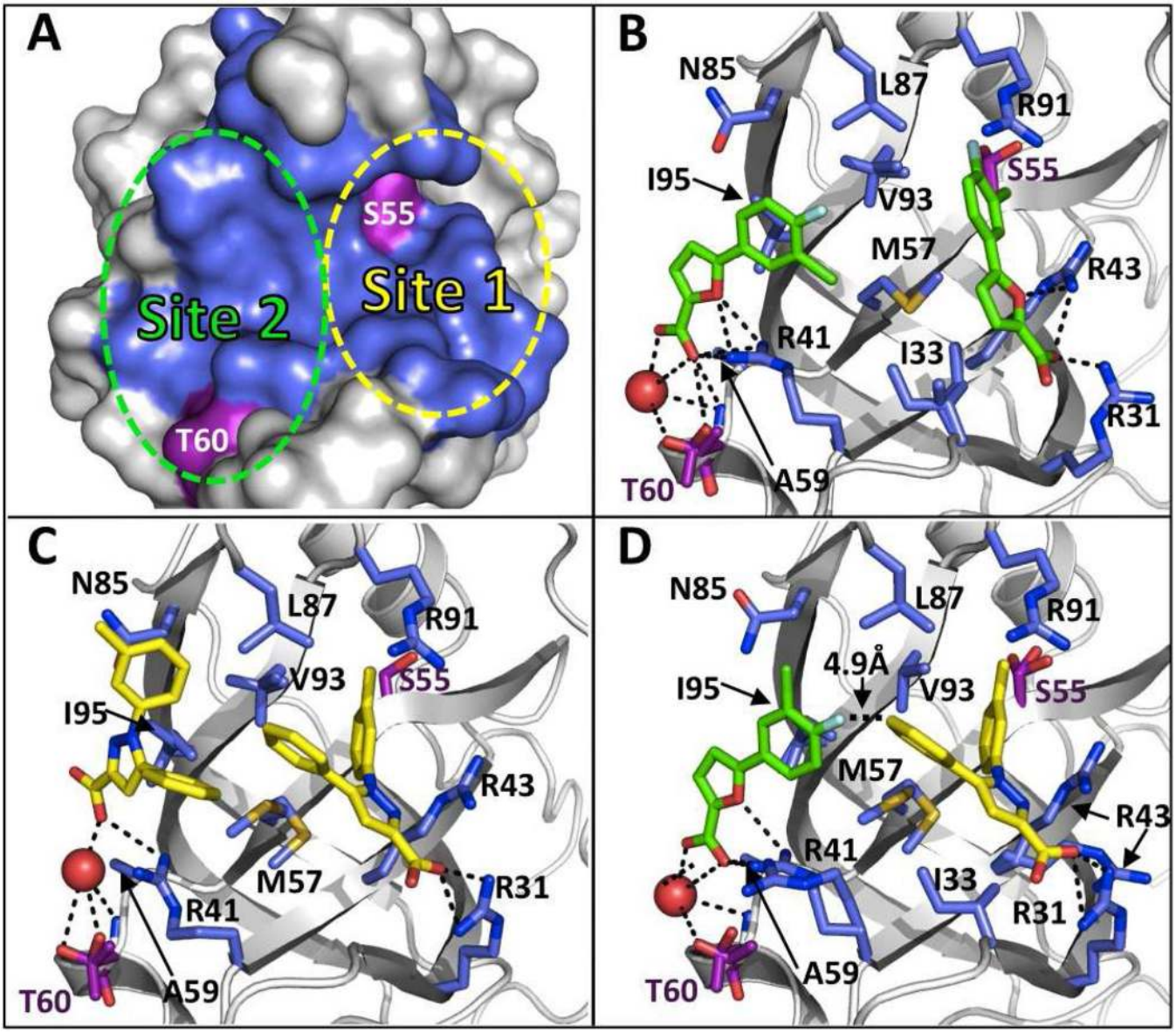

Figure 3.

X-ray crystal structures of RPA70N in complex with small molecule hits. Key water molecules are represented by red spheres. Hydrogen bonds are represented by black dashed lines. Amino acids used as reports in the NMR-based screen for binding to Site-1 (S55) and Site-2 (T60) are colored in magenta. Residues within 3Å of the binding sites are colored in blue. (A) Surface depiction of the basic cleft with Site-1 (S55) and Site-2 (S60) labeled. Fragment **2** (B) and compound **4** (C) bind to both sites. (D) Both compounds can simultaneously occupy the basic cleft as illustrated in the ternary crystallography complex.

NIH-PA Author Manuscript

NIH-PA Author Manuscript

NIH-PA Author Manuscript

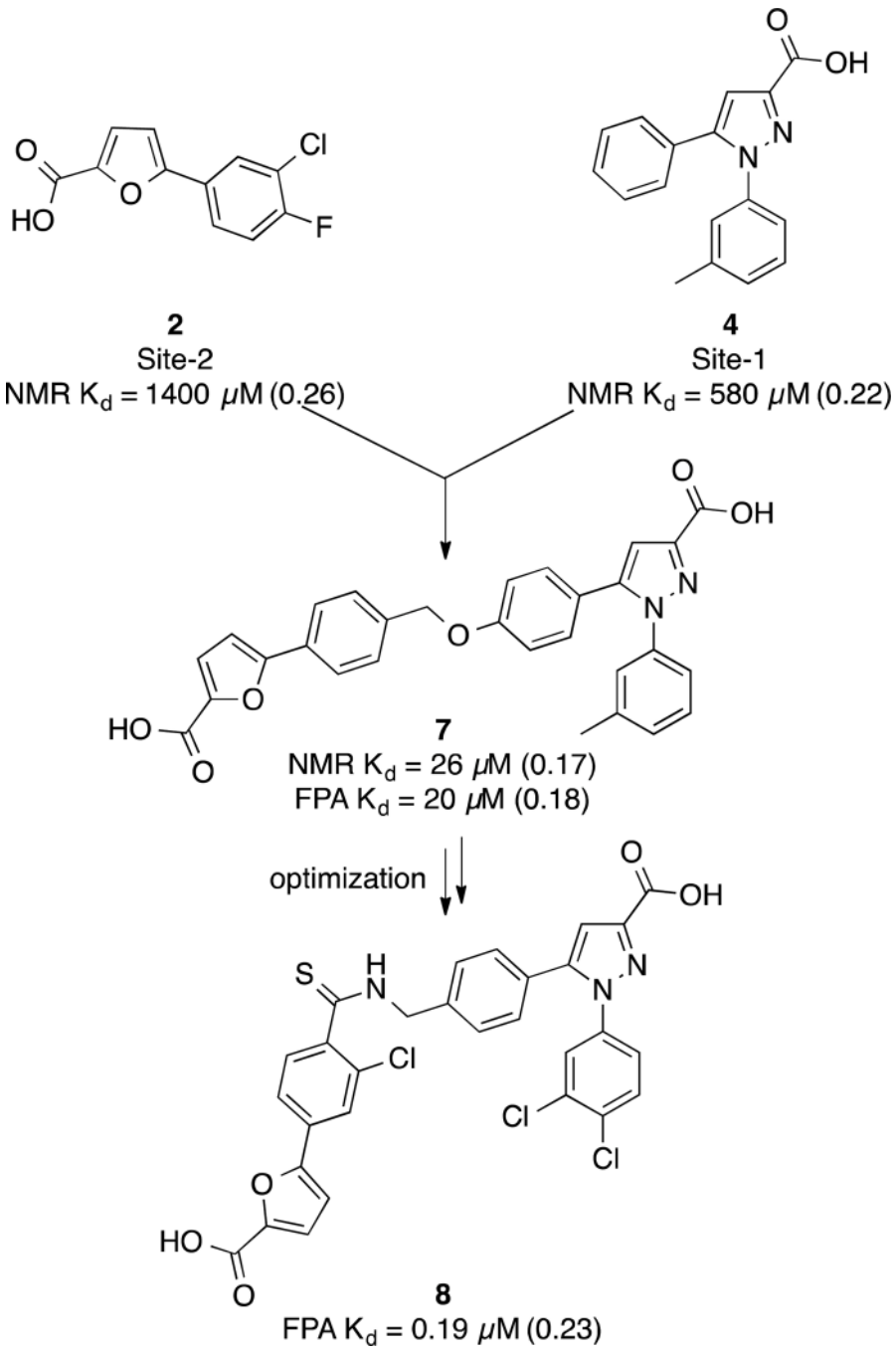

Figure 4.

Overview of the linking strategy and subsequent optimization to design high affinity RPA70N inhibitors. NMR titrations were used to measure weakly bound fragments, while an FPA assay was employed to measure the affinity of the linked compounds. LEs are in parentheses.

NIH-PA Author Manuscript
NIH-PA Author Manuscript
NIH-PA Author Manuscript

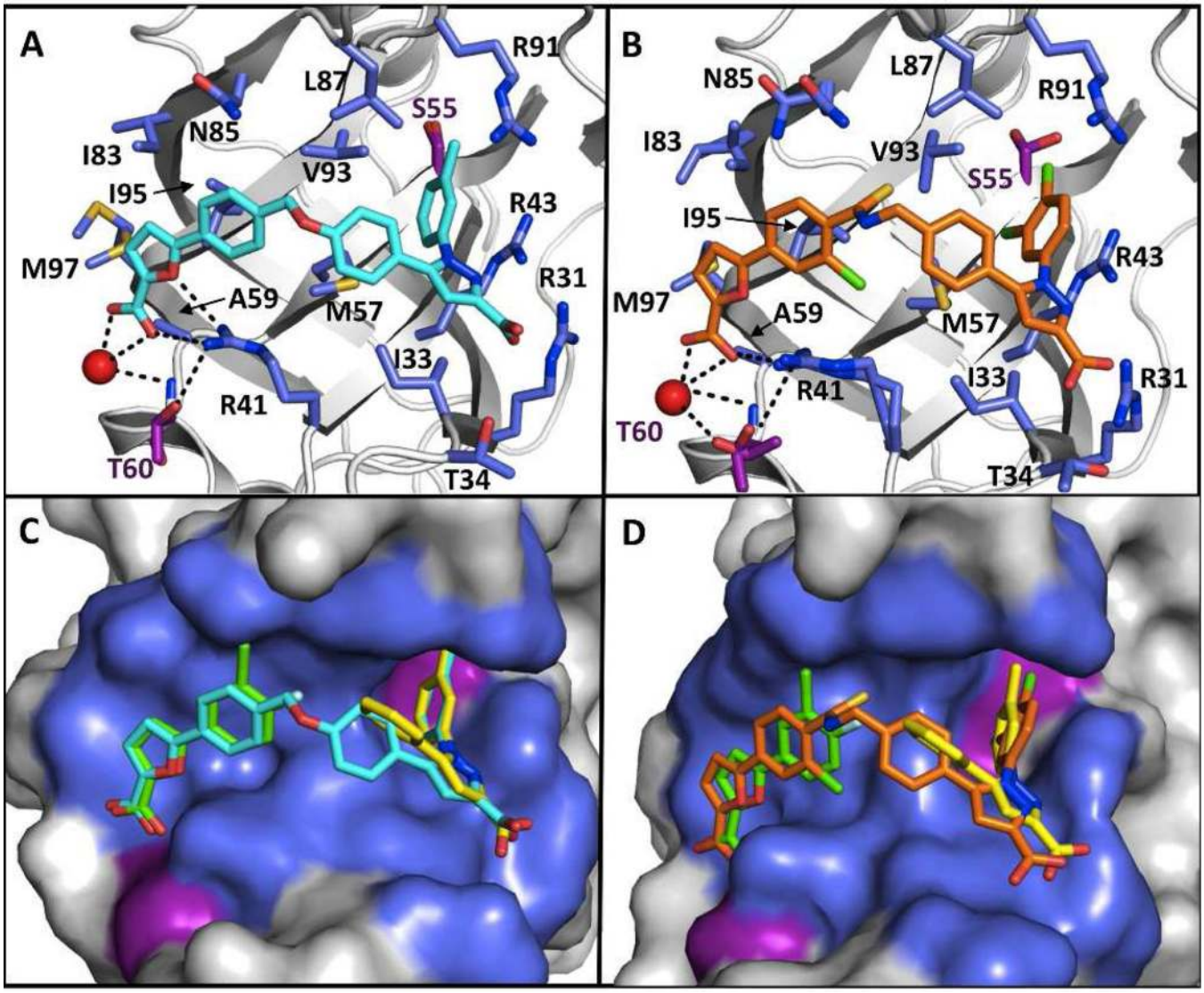

Figure 5.

X-ray co-crystal structures of linked molecules in complex with RPA70N. Key water molecules are represented by red spheres. Hydrogen bonds are represented by black dashed lines. Amino acids used as reports in the NMR-based screen for binding to Site-1 (S55) and Site-2 (T60) are colored in magenta. Residues within 3Å of the binding sites are colored in blue. (A) Compound **7** and (B) compound **8** when bound to RPA70N. (C) Compound **7** and (D) compound **8** overlain with fragment **2** and compound **4**.

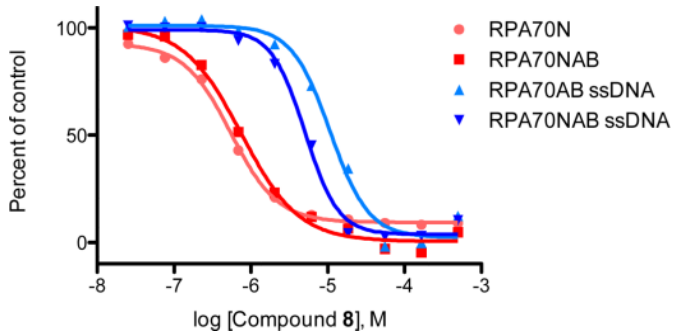

Construct	Probe	IC_{50} (μM)	K_d (μM)
RPA70N	ATRIP2	0.601	0.19
RPA70NAB	ATRIP2	0.753	0.323
RPA70NAB	ssDNA	5.127	2.501
RPA70AB	ssDNA	10.905	5.399

Figure 6.

Compound **8** binds to RPA70N with 10- to 20-fold selectivity over other OB-fold domains. Compound was tested for the ability to displace FITC-ATRIP2 from RPA70N (light red) or RPA70NAB (red). Similarly, compound was examined for displacement of FITC-ssDNA from RPA70AB (light blue) or RPA70NAB (blue). Anisotropy values were normalized to % of control for each set of assay conditions to allow for visualization on the same graph. FPA-derived IC_{50} and K_d values for the displacement of the indicated probe by **8** are indicated.

NIH-PA Author Manuscript
NIH-PA Author Manuscript
NIH-PA Author Manuscript

NIH-PA Author Manuscript

NIH-PA Author Manuscript

NIH-PA Author Manuscript

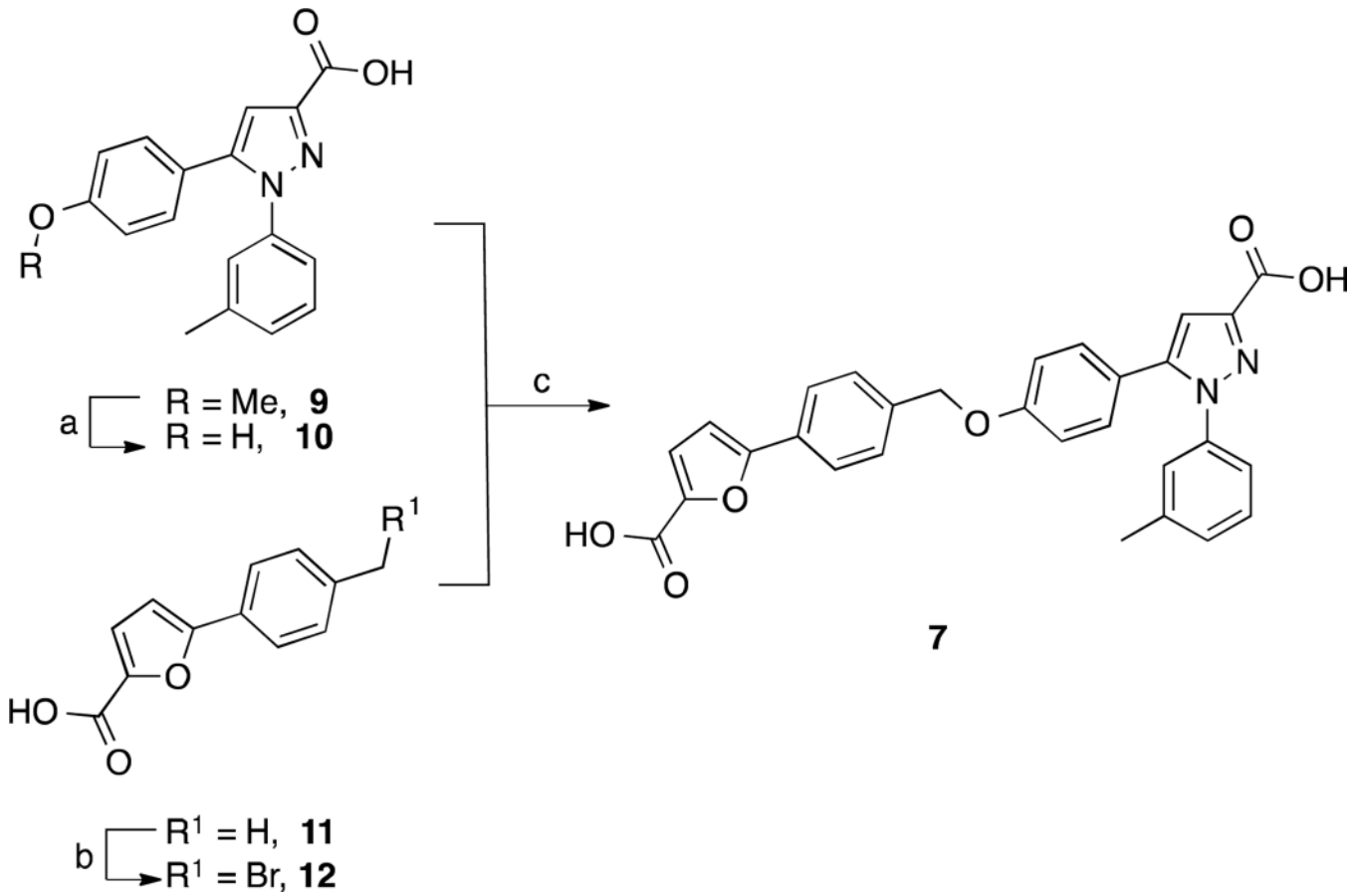

Scheme 1.

Synthesis of linked compound **7**.a

[a]Reagents and Conditions: a) BBr_3, DCM, 0 °C, 62%; b) NBS, AIBN, CCl_4, reflux, 87%; c) K_2CO_3, DMF, 25%.

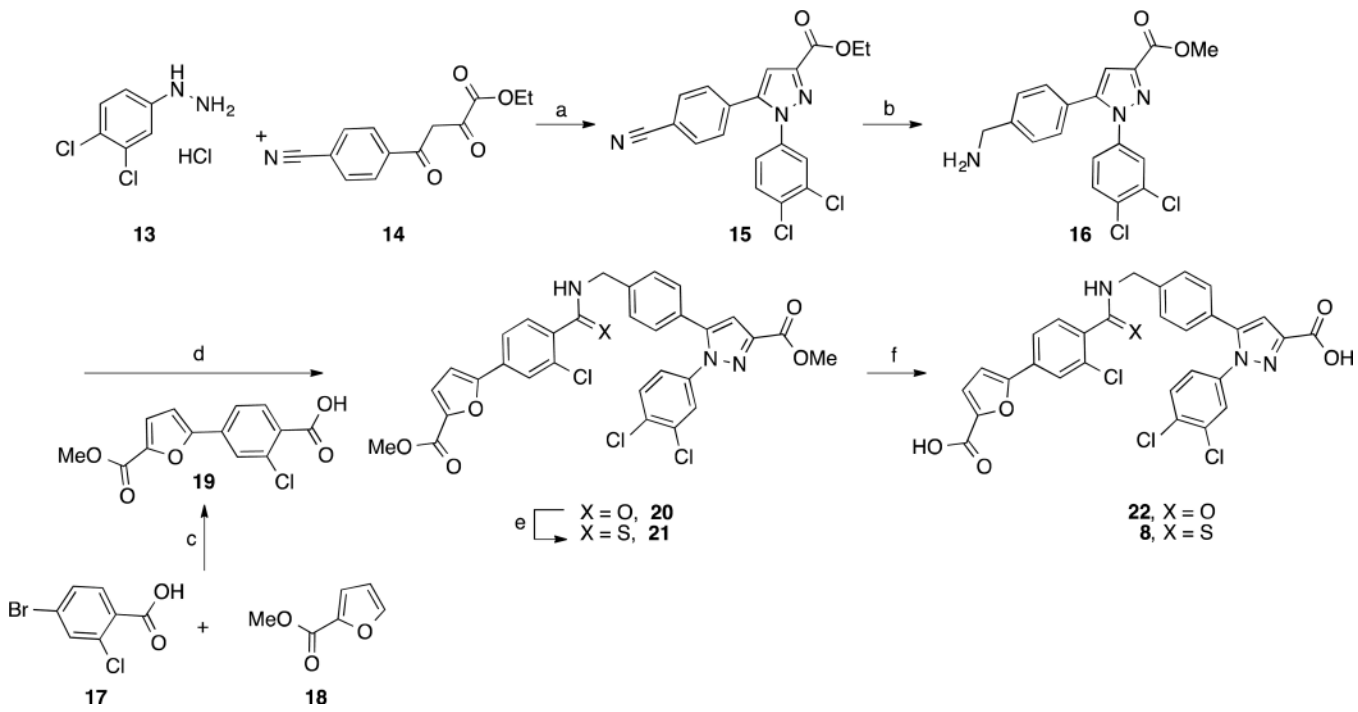

Scheme 2.

Synthesis of linked compounds **8a** and **22**.a

[a]Reagents and Conditions: a) EtOH, 120 °C, 30 min, μwave, 76%; b) 2 M NH_3 in MeOH, cat. Raney nickel, 71 %; c) $Pd(OAc)_2$, KOAc, DMA 100 °C, 30 min, μwave, 41%, d) EDC, HOBt, DIPEA, DMF, rt, 12h; e) Lawesson's reagent, THF, 140 °C, 30 min, μwave; f) 2M LiOH, THF, 120 °C, 10 min, μwave, 20% (two steps) for **22**, 28 % (three steps) for **8**.

NIH-PA Author Manuscript NIH-PA Author Manuscript NIH-PA Author Manuscript

NIH-PA Author Manuscript

NIH-PA Author Manuscript

NIH-PA Author Manuscript

Table 1

Summary of the NMR-based fragment screen against RPA70N.

Total number of screened fragments	14,976
Number of confirmed hits	149
Hit rate	1%
Fragments that bind to both sites	81
Fragments that bind exclusively to Site-1	52
K_d range for Site-1[a]	630–5000 μM
Best ligand efficiency (LE) at Site-1[b]	0.35
Fragments that bind exclusively to Site-2	16
K_d range for Site-2[a]	490–5000 μM
Best ligand efficiency (LE) at Site-2[b]	0.28

[a] Site-1 and Site-2 binding was determined based on the observed chemical shift changes of Ser55 and Thr60 signals, respectively, as observed in heteronuclear correlation NMR spectra.

[b] Ligand efficiencies (LE) were calculated according to the equation LE = (1.4 × pK_d / N) where N is the number of non-hydrogen atoms.[30]